J. Fluid Mech. (1984), *vol.* 149, *pp.* 385–401
Printed in Great Britain

Characteristics of a double-diffusive interface at high density stability ratios

By T. A. NEWELL

Department of Mechanical and Industrial Engineering, University of Illinois at Urbana–Champaign, 1206 West Green Street, Urbana, IL 61801

(Received 3 March 1983 and in revised form 6 July 1984)

A thermohaline diffusive interface at large density stability ratios has been studied experimentally. Several interesting characteristics have been found. First, using a transient experiment technique, a transition from boundary-layer to core-region-dominated transport has been observed. Secondly, interface growth can occur through a series of steps owing to a sharp transition to a region with large interface growth rates. Thirdly, hysteresis occurs within the large density stability ratio region. Finally, the property-transport flux ratio increases as an interface switches from boundary- to core-dominated transports.

1. Introduction

Turner (1965) first reported measurements of heat and salt transport across a double-diffusive interface using a two-layer, bottom-heated experiment. Many interesting features were observed with this experiment. Heat transport appeared to be a function of the density stability ratio R_ρ defined as

$$R_\rho \equiv \frac{\beta \Delta S}{\alpha \Delta T},$$

where $\Delta S \equiv$ salinity difference across an interface, $\Delta T \equiv$ temperature difference across an interface, $\beta \equiv$ saline expansion coefficient and $\alpha \equiv$ thermal-expansion coefficient. Also, the ratio of salt to heat transport diminished as R_ρ increased, but was observed to be constant for R_ρ greater than two. The results are important to areas such as oceanography and engineering. Within oceanography, such layers have been observed and are believed to be important in ocean transports of heat and salt. Within an engineering context, salt-gradient solar ponds have a man-made diffusive interface maintained.

Since Turner's first experiment, several other investigations have been made. Verifications of Turner's results have been made by Crapper (1975) and Marmorino & Caldwell (1976). Crapper repeated Turner's experiment with a more closely controlled apparatus. In addition to verifying Turner's results, Crapper made measurements of the diffusive interface thickness. Marmorino & Caldwell used a different approach from Turner by using a tank that maintained constant-heat-flux boundaries at the top and bottom of the tank, thus approaching a thermal steady-state condition. Their heat-transport results agree with those of Turner, indicating that rundown experiments can behave as if they are passing through a series of quasi-equilibrium steps. Marmorino & Caldwell found an additional feature of the salt–heat-transport relationship. At heat-flux values similar to those used by Turner and Crapper, a transport ratio of similar value was determined. At lower heat flux values, however,

the transport ratio appears to increase. The heat-flux range over which this change occurs is one that is relevant to solar ponds.

Other researchers have used different components for studying double-diffusive convection across a diffusive interface. Shirtcliffe (1973) used sugar and salt, while Takao & Narusawa (1980) used three different solutes with heat. While transport rates for these cases were different from the thermohaline case, a significant feature of these experiments is that the characteristics of the convection are similar. In all cases, transport of the destabilizing component (analogous to heat in the thermohaline case) was found to be dependent on R_ρ. Also, two regimes can be identified which are associated with the transport ratio of the two components. At low R_ρ, interface stability is low and convective motions increase the transport of the slower diffusing component relative to the faster diffusing component. As R_ρ increases, a second regime is encountered where the transport ratio is not dependent on R_ρ.

Experimental studies have given rise to a basic model configuration for the convection process across an interface. An interface is assumed to be composed of a core region that is bounded on either side by unstable boundary layers. Three regimes of operation may be identified with this model. First, at low R_ρ the diffusive core region is very thin and direct interaction appears to occur between the boundary layers. At intermediate R_ρ the core grows and direct boundary layer communication diminishes. The boundary layers are still a dominant factor governing property transport. As R_ρ increases further, the core region grows thicker and becomes the main barrier to property transport.

Previous diffusive interface results have been presented only for the low- and intermediate-R_ρ regimes. Experiment size has been a limiting factor, because large R_ρ values increase the interface thickness to a significant fraction of the total container depth. Direct interaction of the interface with side boundaries, mixed-layer property depletion and significant property retention by the interface relative to the mixed layers are some of the difficulties encountered in large-R_ρ ranges. The present experiment is larger than previous experiments and reduces the significance of the above problems. The experiment has been operated in the intermediate regime in order to compare results with previous investigations. Operation in the large-R_ρ regime has indicated several interesting features. Among these features are:

(1) interface growth under adverse temperature gradients;

(2) transition zone between intermediate- and large-R_ρ regions;

(3) bounded region in which neither interface growth nor erosion occurs;

(4) an apparent path which cyclic interfaces (e.g. seasonal solar-pond variations) may follow.

A model that represents ideal interface growth and thermal equilibration when R_ρ is large has been formulated. The model is a core-region model which complements Linden & Shirtcliffe's (1978) boundary-layer model and serves as a reference case for comparison with experiment results.

2. Experimental apparatus and operation

The present experiment is basically a large-scale version of Turner's (1965) original apparatus. Figure 1 is a schematic of the experiment. The main difference between this device and most previous experiments is that a flat-plate heat exchanger is used for bottom heating instead of a constant-heat-flux device. A tank with temperature control and an electric heating element is connected to the heat exchanger. A pump circulates the heating water to the heat exchanger. In addition to bottom heating,

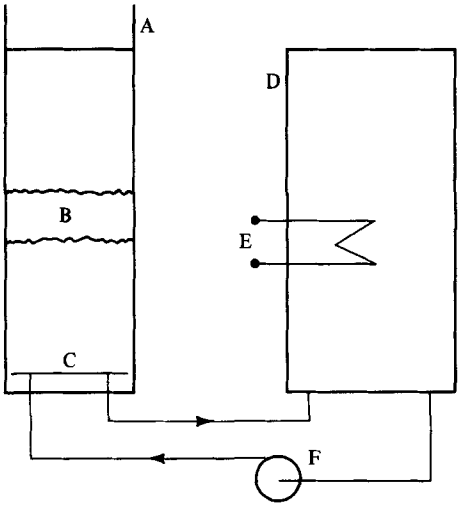

FIGURE 1. Schematic of test facility: A, test tank; B, diffusive interface; C, flat-plate heat exchanger; D, auxiliary heating tank; E, electric heating element; F, circulation pump.

three metal-halide vapour lamps (1200 W each) can be used for radiant tank heating. Present results use only bottom heating or top cooling.

The tank is a self-supporting tube made of PVC (polyvinylchloride). Height is 3 m, diameter is 0.6 m, and wall thickness is 0.635 cm. The tank bottom is 2.54 cm thick Plexiglas. Fibreglass insulation surrounds the tank sidewall, and styrofoam insulation is used on the tank bottom. Sidewall heat conductance is 0.284 W m^{-2} C^{-1}. Sidewall energy losses are typically 10–20 % of energy transport through the interface region. These losses are accounted for in heat-transport calculations. Vertical heat transport through the tank sidewall is estimated to be less than one percent, and has been neglected.

Temperature measurements are made with thermocouples. A stationary thermocouple is located in the midregion of each mixed layer. A manually traversing thermocouple probe is used for interface temperature-profile measurements. Also, tank bottom and top are traversed to detect regions of temperature inversions. No temperature inversions are detected in any of the experiment runs. Temperature traversing scans are made in both upward and downward directions. Within the accuracy of thermocouple sensitivity (± 0.1 °C), no differences are observed and no systematic errors are apparent. Because the rate of change of density stability ratio varies depending on the R_ρ region, the temperature scan frequency varies. At low R_ρ values (4–12), mixed-region temperature recording intervals are of the order of 5 min. For larger R_ρ values, hourly mixed zone temperatures are recorded, and approximately two temperature traversing scans per day are made. Properties were evaluated from the *Saline Water Conversion Engineering Data Book* (1971).

Two methods were used for determination of interface heat transport. When the interface thickness was less than two centimetres, a transient energy analysis was used on the bottom mixed layer. This is similar to the technique used by Turner (1965) and Crapper (1975). A stable core region was discernible with temperature probe traversing as interface thickness increased. Marmorino & Caldwell's (1976) graphical procedure was used for evaluating the temperature gradient within thicker interfaces. Where both methods were applicable (usually if $10 < R_\rho < 12$), both were used.

Salt concentration was measured in two ways. *In situ* conductivity probes

(Beckman model K10Z20 for the top zone and model K100Z20 for the bottom zone) were connected to a YSI model 32 conductance meter. Surface zone samples were also collected (approximately one per day) in order to check *in situ* probe calibrations. Salinity levels have been less than 5% and temperature levels less than 45 °C for all tests performed. An initial series of experiment runs (numbers 1–11) lacked salinity profile information within the interface.

A second series of experiment runs (numbers 13–16) was made in order to further substantiate the results from the initial experiment series. For the second series, a dual-needle conductivity probe was fabricated. The probe consists of two 0.05 mm platinum wires sealed in separate 1 mm capillary glass tubes. The glass tubes were heated and necked down at the electrode tip. The electrode-tip spacing was approximately 1 mm. A standard platinizing solution was used to coat the electrode tips. The probe was calibrated *in situ* before each traverse using the upper and lower mixed-zone conductivity probes. Approximately once per week, the dual-needle probe calibration was checked using a series of standard solutions. A thermocouple was also mounted with the dual-needle electrode. The thermocouple was in the same horizontal plane as the electrodes and was spaced approximately 15 mm away from the electrodes.

Interface thickness was evaluated using Marmorino & Caldwell's procedure A best-fit line drawn through interface temperature scan data was extended to upper and lower mixed-layer temperatures. For the most part, accuracy of this method was quite good, since almost all data exhibited linear temperature profiles. Most inaccuracies from this method were based on the profile shape near the mixed-layer region of the interface. For example, sometimes the temperature-profile data proceeded almost directly to the mixed-zone temperatures. In other profile data in which the same midinterface temperature gradient was observed, the temperature approach near mixed-zone regions had a more gradual slope. Usually, temperature profiles were quite linear over at least 75% of the interface region. Variation of interface thickness due to mixed-zone region profiles is estimated to be within ± 1 cm. An example of the error incurred due to a nonlinear temperature profile is described in a later section.

The basis for the experimental procedure was the following. All changes imposed on the interface region were to occur at a rate which would approximate thermal steady-state. That is, interface temperature profiles display linearity. This is in contrast with transient experiments with large gradient zones, where large heat-flux variations are imposed, resulting in nonlinear temperature profiles. The limiting case of very high heat flux imposition on a density gradient was that investigated by Turner (1968), Shirtcliffe (1969) and Huppert & Linden (1979). At high heat-flux values penetration of the temperature front into the interface is small relative to the advancing mixed layer. Also, a high heat-flux case leads to the formation of a layered structure. At moderate heating-rate variation, such as used in the experiments at Purdue University (see Lewis, Incropera & Viskanta 1982; Poplawsky, Incropera & Viskanta 1981), layered structures are not formed; however, quite-nonlinear temperature profiles are observed. The present interface was subjected to a slower variation of heat flux so that the temperature profile remained linear. Under this condition, interface growth and erosion was observed.

Using the above procedure, bottom heating or top cooling was used to impose a heat flux on the interface. The interface observed was symmetrical, and showed no obvious effects to differentiate bottom heating and top cooling. No temperature fluctuations within the mixed regions (± 0.1 °C) were observed until the edge of the

Run	ΔT_i	ΔT_f	ΔS_i	ΔS_f	δ_i	δ_f	Comments
1	11.1	2.6	4.5	4.4	7	14	Initial temperature difference imposed through bottom heating. Heating terminated before significant interface erosion occurred. Interface proceeded toward thermal equilibrium. Total water depth was 2.4 m.
2	13.4	2.7	4.4	4.1	3	16	Same procedure as above, except initial bottom heating was imposed until the interface was fully eroded.
5	10.5	2.0	3.0	2.8	3	18	Same procedure as run 2. Top surface was insulated with 4 cm of styrofoam.
6	8.6	2.0	2.7	2.7	7	14	Same procedure as run 1. Top-surface insulation was used.
7	2.4	1.9	2.7	2.6	12	14	At the conclusion of run 6 insulation was removed from the top surface. Surface cooling resulted in decreasing/increasing of interface R_ρ. Insignificant erosion/growth observed. Maximum ΔT was 5.5 °C.
9	6.1	1.2	2.0	1.4	2	12	Same procedure as run 2.
11	9.5	2.2	2.7	2.4	11	9	Same procedure as run 1. Total water depth 1.2 m (half as deep as previous runs).
13	2.4	1.6	3.9	3.9	12	16	Conclusion of a run similar to run 2. Total tank depth 2.4 m. Top surface insulated. Begins series of runs with interface salinity data.
14	1.9	4.9	3.9	3.9	15	14	At the conclusion of run 13, surface
15	4.9	4.9	3.9	3.9	14	18	insulation was removed in a similar
16	4.7	2.2	3.9	3.7	25†	11	manner to run 7. Run 14 represents the R_ρ decrease portion of the process. Run 15 is the R_ρ increasing process. Bottom heating of tank was maintained until interface erosion complete. After erosion, bottom heating discontinued and interface growth monitored.

† Initial bottom heating rate resulted in an artificially high value for interface thickness using the procedure outlined. Interface thickness based on temperature and salinity probe measurements was 16 cm. See §3.4.

TABLE 1. Description of experimental runs. Runs 2, 5, and 9 are described in §3.1, runs 1, 6, 7, and 11 are described in §3.2, runs 13, 14, 15, and 16 are described in §3.3. $\Delta T_i \equiv$ initial temperature difference for a run (°C), $\Delta T_f \equiv$ final temperature difference for a run (°C), $\Delta S_i \equiv$ initial salinity difference for a run (% wt fract.), $\Delta S_f \equiv$ final salinity difference for a run (% wt fract.), $\delta_i \equiv$ initial interface thickness for a run (cm), $\delta_f \equiv$ final interface thickness for a run (cm).

interface region was approached. At this region temperature fluctuations depended on interface stability. Low R_ρ values (4–6) produced fluctuations of the order of the interface temperature difference. At high R_ρ values boundary fluctuations dropped to the level of temperature-measurement sensitivity. The lack of temperature fluctuations across the mixed zones indicates that direct communication between heating (cooling) surface thermals and interface thermals may not have occurred.

Table 1 provides a brief summary of the experimental runs to be described. Experimental runs 1–11 form the first series. Although several of the runs were

performed at the conclusion of a previous run (i.e. using the resulting mixed-zone property levels of the previous run), these runs were separate. The second series of experiments (runs 13–16) is actually one long run which forms a continuous sequence of the characteristics observed in the first series. Detailed salinity-profile information was obtained in the second series, and is used to discuss relative transports of salt and heat across the interface.

3. Experimental results and discussion

Four main features of the large-R_ρ interface region will be presented. First, the transition between intermediate- and large-R_ρ regimes will be shown to be quite distinct. Secondly, the fluxes of heat and salt are not uniquely determined by R_ρ. Thirdly, the interface may evolve in a cyclic manner relevant to systems such as solar ponds that undergo seasonal variations. Finally, the ratio of salt transport to heat transport increases as an interface moves into the large-R_ρ regime.

3.1. *Intermediate–large-R_ρ transition*

The boundary-layer transport models of Linden & Shirtcliffe (1978) and Lindberg (1971) show that the heat-flux ratio tends toward zero as R_ρ approaches the square root of the high- to low-diffusivity ratio. As reasoned by Linden & Shirtcliffe (1978), the trend is because the interface boundary layers can no longer be modelled by a steadily fluctuating system. That is, when the boundary layers destabilize, they do not erode back to their initial state. Therefore transient development of the interface is important and must be accounted for.

Three experimental runs are shown in figure 2. Experimental runs 2, 5 and 9 consisted of approximately 2.4 m total tank depth with 1.2 m depth per mixed layer. Average salt-concentration differences for runs 2, 5 and 9 were 4.5, 3 and 1.5% respectively. Because the experiments were not operated in the variable regime ($R_\rho < 2$ for the thermohaline systems), the variation of salt-concentration difference throughout the course of any experiment was small. All three runs were made in a similar manner by initially heating the tank from below until an R_ρ of approximately 4 was attained. Then heating was discontinued and the system was allowed to approach thermal equilibrium. The water surface for experiment 5 was insulated with 4 cm of styrofoam insulation in order to change the thermal-equilibration rate. The other two runs were open to ambient laboratory air conditions.

Solid data points in figure 2 used transient energy analysis, while hollow data points used interface data. The heat flux ratio $H/H_{\rm sp}$, is the reference case defined by Turner (1965) for interface heat flux relative to that across a perfectly conducting membrane. It is evaluated as

$$\frac{H}{H_{\rm sp}} = \frac{\mathrm{d}T}{\mathrm{d}z}\Big/\left[0.085\left(\frac{g\alpha}{K_T\nu}\right)^{\frac{1}{3}}(\Delta T)^{\frac{4}{3}}\right],$$

where $\mathrm{d}T/\mathrm{d}z \equiv$ interface temperature gradient, $g \equiv$ gravitational acceleration, $K_T \equiv$ thermal diffusivity and $\nu \equiv$ kinematic viscosity. A transition zone is sketched on figure 2 between R_ρ values of 6–10. The actual width of this region is the boundary between unique $H/H_{\rm sp}$ operation (intermediate R_ρ) and non-unique $H/H_{\rm sp}$ operation (large R_ρ).

Figure 2 also has several curves sketched on it. Curves A and B are empirical curve fits to previous investigators' data which have been extrapolated to large R_ρ values. Curve A is Huppert's (1971) fit for Turner's (1965) data. Curve B is Marmorino & Caldwell's (1976) curve fit of their own data. As indicated on figure 2, neither of these

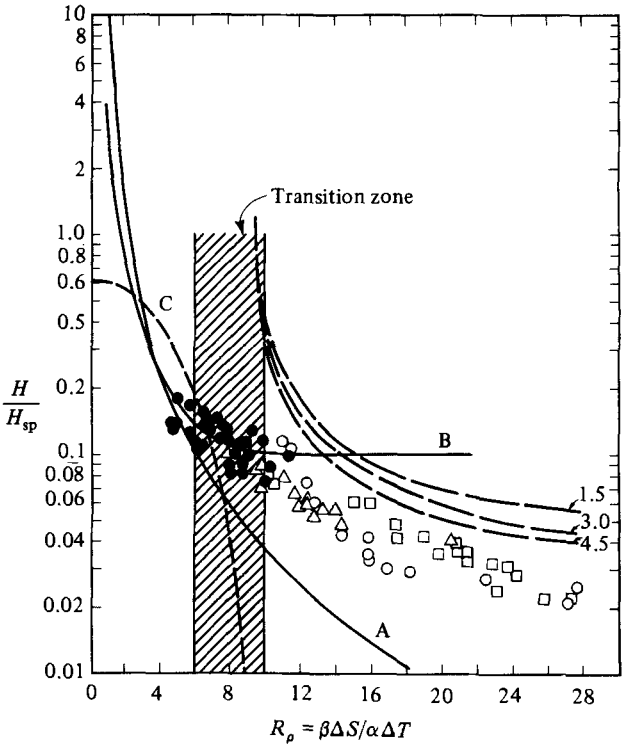

FIGURE 2. Plot of interface heat-flux ratio H/H_{sp}, versus interface density stability ratio for a total tank depth of 2.4 m: ○, experiment 2 (4.5% interface concentration difference); □, experiment 5 (3%); △, experiment 9 (1.5%).

curves should be extrapolated past the data region from which they have been derived.

Curve C is from Linden & Shirtcliffe's (1978) boundary-layer model. H/H_{sp} from their model is given as

$$\frac{H}{H_{sp}} = \frac{1}{\pi^{\frac{1}{3}}} \frac{(1-\tau^{\frac{1}{2}}R_\rho)^{\frac{4}{3}}}{(1-\tau^{\frac{1}{2}})^{\frac{1}{3}}}, \tag{3.1}$$

where $\tau \equiv$ ratio of salt to thermal diffusivity. H/H_{sp} goes to zero as R_ρ increases to $\tau^{-\frac{1}{2}}$ (approximately 9.5 for thermohaline interfaces). In real systems H/H_{sp} does not drop sharply when R_ρ exceeds $\tau^{-\frac{1}{2}}$. Instead, transient interface growth can occur. An ideal model has been derived, and is plotted in figure 2. The model is based on two assumptions which are limits describing interface growth and heat transport. These assumption are:

(1) interface growth occurs at a rate governed by the slower-diffusing component;

(2) heat transport occurs only between the mixed layers; this represents the fastest approach to thermal equilibrium.

The first assumption is an idealization, which assumes that, as the temperature profile outgrows the salt profile and destabilizes, it does not erode back to its original position. That is, the progress made by the growing salt profile is not erased. The thickness of the interface based on salt-diffusion growth is assumed to be the only resistance to heat transport. Therefore the model is a core-dominated transport model. At the transition zone where boundary-layer dominance is assumed to be replaced by core dominance, the initial core thickness is assumed to be zero. Because

heat transport is based on the thermal conductivity and thickness of the interface, H/H_{sp} will be infinite at this point. The heat transport between the two mixed layers is governed by

$$\frac{d\Delta T}{dt} = -\frac{2K_T}{D\delta}\Delta T, \tag{3.2}$$

where $t \equiv$ time, $D \equiv$ depth of a mixed layer and $\delta \equiv$ interface thickness. An estimate of interface thickness is based on the slope at the midplane of two layers of different property levels brought into contact and communicating by diffusion. The midplane slope is extended until it intersects property values equal to the initial property conditions. Under this assumption, the interface thickness is

$$\delta = 2(\pi K_S t)^{\frac{1}{2}}, \quad \text{where } K_S \equiv \text{saline diffusivity}.$$

Solving (3.2) with this condition, and using this result in conjunction with the definitions for H/H_{sp} and R_ρ yields

$$\frac{H}{H_{sp}} = \left[0.085\,\pi^{\frac{3}{2}} D\tau \ln\frac{R_\rho}{R_{\rho i}}\right]^{-1} \left(\frac{g\beta\Delta S}{\nu K_T}\right)^{-\frac{1}{3}} R_\rho^{\frac{1}{3}}. \tag{3.3}$$

Curves for concentration differences of 4.5, 3 and 1.5% have been plotted for comparison with experiments 2, 5 and 9. The $R_{\rho i}$ value is the integration constant from (3.2), and is designated as the time when transition from boundary-layer dominance to core dominance occurs. $R_{\rho i}$ is assumed to be $\tau^{-\frac{1}{2}}$ where Linden & Shirtcliffe's (1978) model goes to zero.

The data and ideal curves shown in figure 2 have similar trends. The ideal curves would have better agreement with the data if a finite resistance for the interface is assumed at $R_{\rho i}$ (at transition the interface thickness δ is 2–3 cm). An interesting feature of large-R_ρ interfaces is the region bounded by the transition zone and the experiment data. Within this region, interface growth and erosion rates are small. As an interface approaches the transition zone, erosion rates increase significantly. As the experimental data of figure 2 are approached, interface growth rates increase significantly.

Subsection 3.2 will provide results from experimental runs which illustrate the lack of erosion or growth within the region bounded by the transition zone and the data of figure 2. Two other features of interface growth are worth considering before these results are presented. First, a plot of interface thickness versus experiment time shown in figure 3 for experiments 2, 5 and 9 indicates possible growth cycles. Time resolution of the data is not sufficient to allow actual determination of growth cycle frequencies for the interfaces. A best-fit line has been drawn through each of the data sets for reference.

A second feature to consider is interface thickness as a function of R_ρ. Figure 4 shows this plot for experiments 2, 5 and 9. The line drawn on figure 4 is obtained from the ideal model, and is given by

$$\delta = \pi^{\frac{3}{2}} D\tau \ln(R_\rho/R_{\rho i}). \tag{3.4}$$

3.2. *Region of slow erosion/growth*

Subsection 3.1 described a series of experimental runs which illustrate growth of an interface. Results are presented in the subsection which support the existence of a region in which either erosion or growth of an interface is much slower than at the bounding regions.

A region of small interface growth or erosion would appear as an approximately

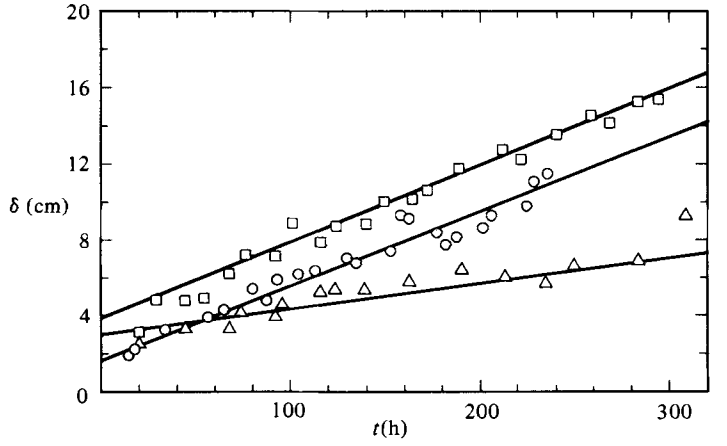

FIGURE 3. Interface thickness versus time for experiments 2, 5 and 9 (symbols are consistent with figure 2 experiment designations).

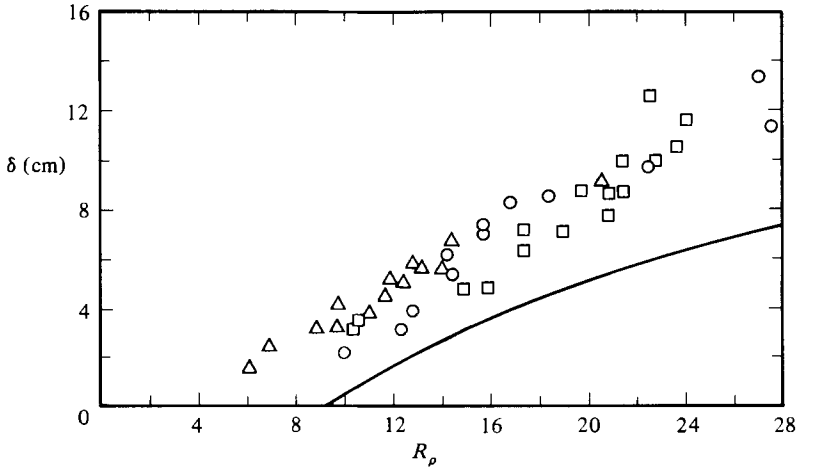

FIGURE 4. Interface thickness versus interface density stability ratio for experiments 2, 5 and 9 and the theoretical interface thickness prediction from (3.4).

horizontal traverse on a plot of H/H_{sp} versus R_ρ. This is true if one assumes salt transport is low enough to result in negligible depletion/addition of salt to the bottom and top mixed layers respectively. Assuming properties are relatively constant and the interface thickness is constant, H/H_{sp} is dependent on the inverse of the interface temperature difference raised to $\frac{1}{3}$ power, while R_ρ is proportional to the inverse of the interface temperature difference. The actual traverse is not strictly horizontal, because both H/H_{sp} and R_ρ are functions of interface temperature difference. However, because H/H_{sp} is more strongly affected by interface thickness (proportional to the inverse of interface thickness), a region of little growth will appear relatively flat compared with regions where interface thickness changes are significant.

Results from four experimental runs are presented in figure 5 for H/H_{sp} versus R_ρ. Two of these runs (experiments 6 and 11) started in the transition region where strong erosion of an interface occurs. Unlike the runs described in §3.1, heating of the bottom layer had been discontinued before the interface was eroded sufficiently for transition to the intermediate-R_ρ region. That is, if heating had been continued on experiments

6 and 11, a nearly vertical movement would have occurred until curves A and B of figure 1 were attained. Discontinuation of heating resulted in an approach towards a thermal equilibrium and large R_ρ values. The four runs show relatively little change of interface thickness for a variety of H/H_{sp} levels. After the experiments traversed a range of R_ρ values, H/H_{sp} began to decrease significantly, indicating interface growth. An interesting feature of the growth is that it begins in a manner consistent with the results of the previous section where the interface began in the intermediate-R_ρ regime.

Experiment 7 pictured on figure 5 is interesting because it was moved in both directions across the slow-erosion/growth region. This movement was achieved by removing the surface insulation at the conclusion of run 6. The top mixed layer was approximately 5 °C warmer than ambient room air. Because evaporative and convective cooling from the tank surface was more efficient than the interface transport, the top mixed layer proceeded to cool. The bottom mixed layer remained relatively warm, and therefore the temperature difference between the two layers increased and R_ρ decreased. The rate of change of top-layer temperature was slow enough such that the condition of thermal steady state (linear interface temperature profiles) was maintained. The experiment lasted 8 days, with approximately 3 days during which R_ρ decreased and 5 days where R_ρ increased.

Figure 6 is a plot of temperature scans for experiment 11. This plot shows both erosion and growth of the interface. The arrow on the plot shows profile direction with respect to time. The temperature profiles are linear throughout most of the interface, and the calculated midplane location of the interface remained within one centimetre. Most of the interface midplane-location variation occurred during the first three data sets (24 h) when the initial temperature gradient was not quite linear. The temperature profile near the upper boundary was steeper than the lower region and resulted in a larger amount of erosion. Total duration of this experiment was 6 days.

Figure 7 shows the variation of interface thickness as a function of R_ρ. Within the transition region erosion of the interface is significant. As an interface exits the transition zone neither erosion nor growth is significant. At larger R_ρ values interface growth becomes significant.

3.3. *Cyclic operation of an interface*

The separation of growth and erosion regions of a diffusive interface can result in a hysteresis when an interface traverses between the two extremes. This is in contrast with the intermediate- and low-R_ρ regimes, where increasing- and decreasing-R_ρ movements are along the same path. A second series of experiment runs was performed to illustrate these characteristics. Detailed salinity-profile data were taken during these runs.

Experimental runs 13–16 are a continuous sequence of runs. Figure 8 is a plot of H/H_{sp} versus R_ρ for these runs. Run 13 was a growth run similar to those shown in figure 2. The surface was insulated and the experiment proceeded until R_ρ was approximately 50. At this point the surface insulation was removed. The top mixed layer was warmer than the ambient air, and, in a manner similar to experiment run 7 (shown in figure 5), R_ρ began to decrease. This decreasing-R_ρ process has been labelled as experiment run 14. As the top mixed layer approached ambient air temperature, R_ρ began to increase. The increasing-R_ρ process was experiment run 15. When R_ρ approached 35 bottom heating was initiated in order to move the interface toward the transition region. Significant interface erosion was observed as the

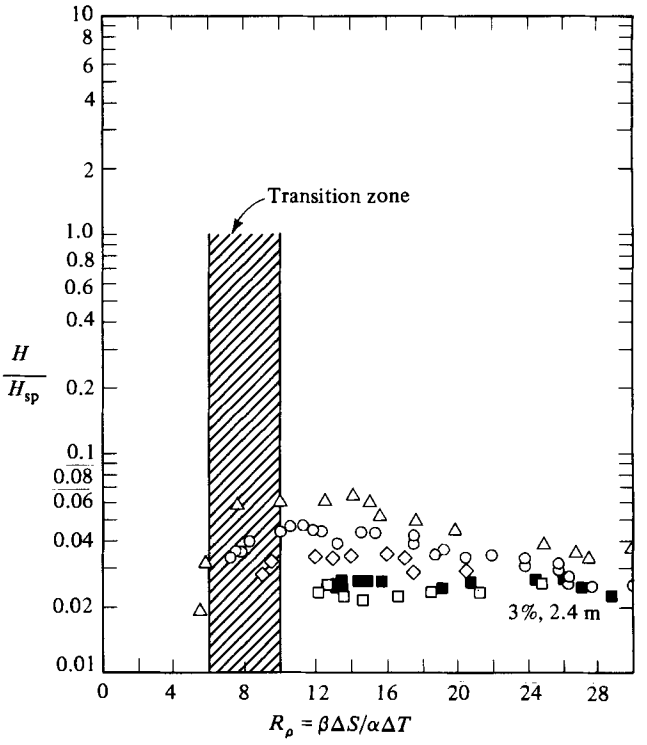

FIGURE 5. Plot of interface heat-flux ratio versus inerface density stability illustrating the region of low interface erosion/growth rates. Experiments 1 (◇), 6 (○), 7 (□, R_ρ decreasing; ■, R_ρ increasing) and 11 (△) all had concentration differences of approximately 3 %. Experiment 11 was 1.2 m deep and the other three were 2.4 m deep.

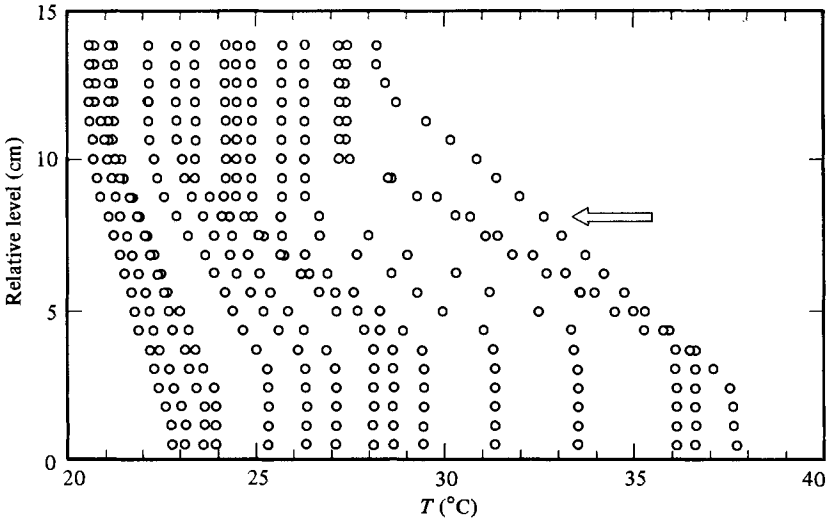

FIGURE 6. Temperature scan profiles from experiment 11 showing interface erosion and growth.

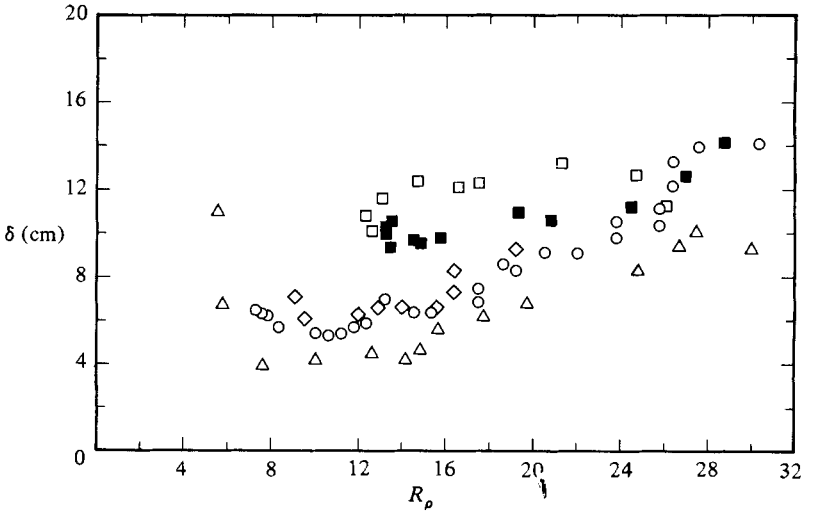

FIGURE 7. Interface thickness versus interface density stability ratio for the experiments described in figure 5.

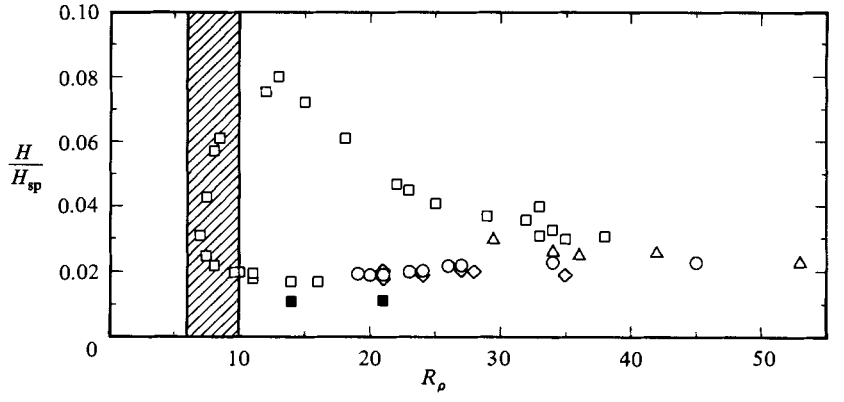

FIGURE 8. Interface heat-flux variations for experiments runs 13 (△), 14 (○), 15 (◇) and 16 (□).

transition zone was entered. The interface continued to erode until its thickness was approximately 3 cm. Bottom heating was discontinued when the interface was fully eroded. The interface grew in a consistent manner as observed in the beginning of the experiment series (run 13).

Temperature and salinity profiles for experiment runs 13–16 indicate a couple of interesting features. Figure 9 shows temperature and salinity data during the growth period of run 13. It is seen that there is no significant difference of interface thickness based on temperature or salt. One should expect a 'double-boundary-layer' structure to exist at the outside edges of the interface. The difference found in boundary-layer thicknesses for salt and heat is less than the spatial resolution of the temperature/salinity probe. In general, for the probe configuration and instrument sensitivities used in this study, salt and temperature changes from mixed-layer property levels were detected at the same position and time.

Figure 10 is a profile taken approximately 2 h after bottom heating was started (end of run 15 and beginning of run 16). The imposed heating conditions were higher

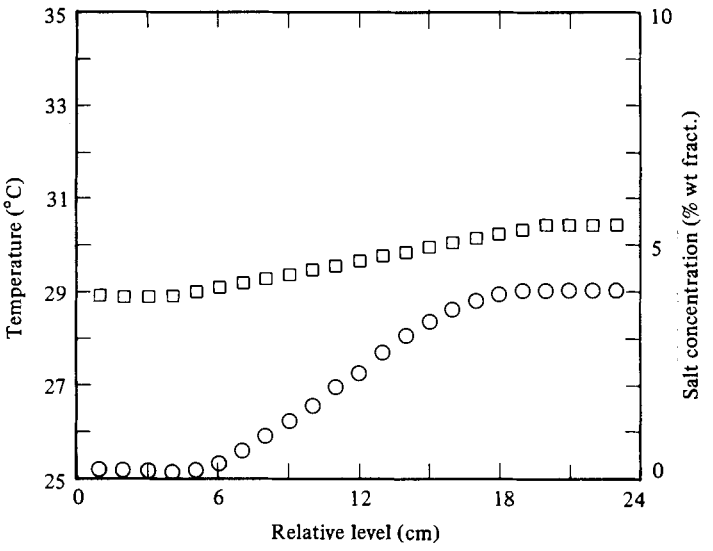

FIGURE 9. Temperature (□) and salinity (○) profiles across the interface during run 13.

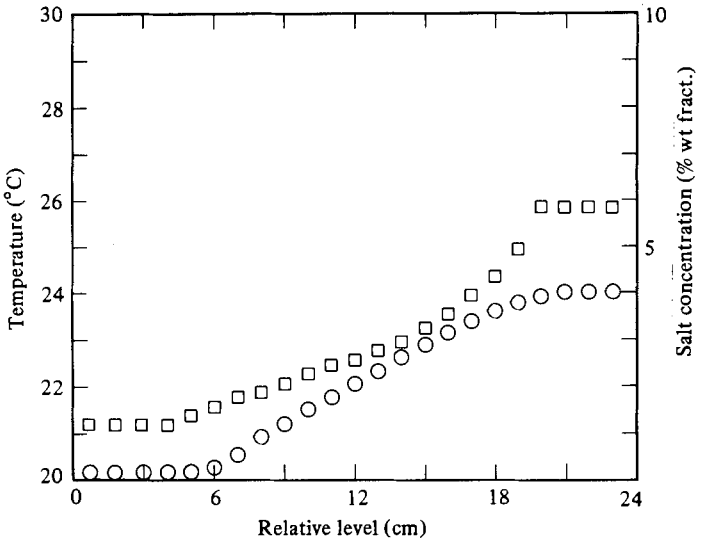

FIGURE 10. Nonlinear temperature profile (□) due to bottom heating at the beginning of run 16 (○, salinity).

than desired, and the resulting temperature profile was very nonlinear. The local increase in temperature gradient was not high enough to cause significant localized erosion. Figure 11 shows profile data approximately one day after heating was begun. The interface had approached a thermal steady-state with a similar overall interface thickness. The salinity profile was stable throughout this process.

The temperature profile shown in figure 10 (and a subsequent reading taken four hours later) yield erroneous information in terms of interface heat flux and thickness. These two data points result in a low H/H_{sp} calculation because the interface temperature difference was high relative to the interface temperature gradient. The two data points are indicated by filled symbols on figure 10. The nonlinear

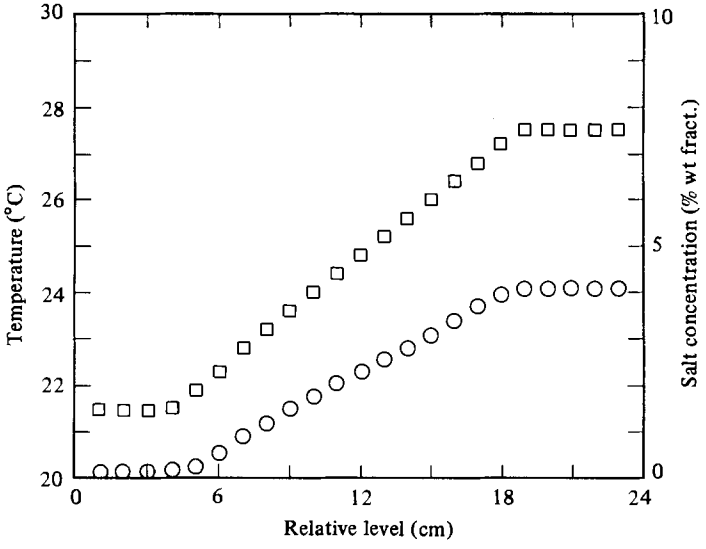

FIGURE 11. Temperature (□) and salinity (○) profiles 24 h after bottom heating was initiated for run 16.

temperature profiles for the two data points also resulted in a larger interface thickness prediction. Figure 12 is a plot of interface thickness for experiment runs 13–16. Regions of growth and erosion are observed. The two data points with significantly nonlinear temperature profiles have filled symbols in figure 12.

Solar ponds may operate under a similar type of cycle. Newell & Boehm (1982) have observed that sodium chloride solar ponds seem to have an operational limit which is reached as a pond heats up through the summer season. The operational limit constrains the maximum temperature difference obtainable across the mixed zones of a solar pond to the salinity difference being maintained. Although a solar pond is not a symmetric interface because of solar-energy absorption within the interface, local conformance to the limiting condition appears to be valid. Within the context of the present paper, the operational limit for solar ponds was found to be at R_ρ values between 7 and 8. That is, as a pond emerges from winter cooling at relatively high-R_ρ values (12–15), R_ρ continually decreases to the operational limit. If a pond were held at this limiting condition for a long time, an increase of H/H_{sp} would occur until the unique path within the intermediate- to low-R_ρ region is attained. At the end of the summer season as solar radiation declines, the pond proceeds back into the large-R_ρ region.

Another indication of the transition barrier between the large- and intermediate-R_ρ regimes may be found in the analysis of Marmorino (1974). In an appendix, Marmorino presents transient results from one experiment. Basically, a two-layer isothermal system would be set up and then heated until equilibrium was achieved. Because Marmorino was interested in the low- and intermediate-R_ρ regions, the initially isothermal system would traverse the transition region. The results shown for Marmorino's experiment 23 indicate that R_ρ rapidly decreases with respect to time until the transition region is approached. In the transition region R_ρ variation slows down significantly. The decrease in R_ρ variation may be attributed to readjustment of the interface in a manner similar to the process shown in figure 8. Because Marmorino maintained a constant heat flux, his system proceeded toward lower R_ρ and ultimately toward destabilization since salt boundary conditions were not maintained.

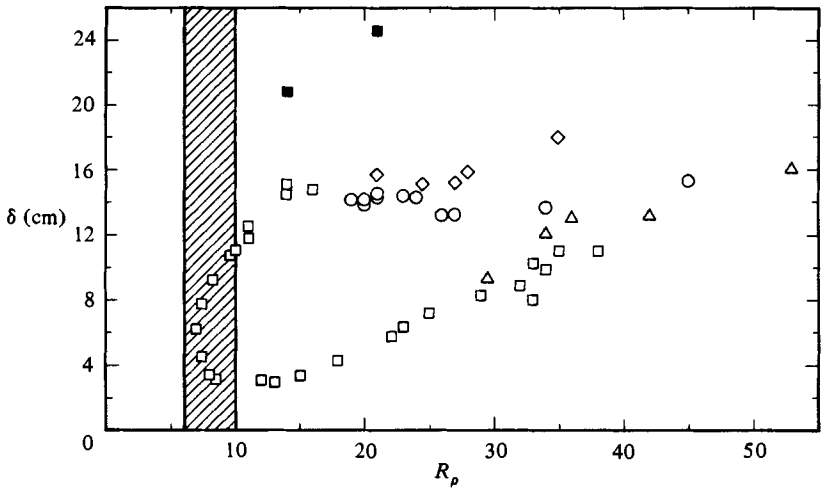

FIGURE 12. Interface thickness for experiment runs 13, 14, 15 and 16.

3.4. *Transport flux ratio*

An interesting and as yet unresolved feature of a diffusive interface is the relative transport of the diffusing components. Turner and Crapper found a variable regime to exist for R_ρ values less than 2. As R_ρ decreases below 2, salt transport increases relative to heat transport. For R_ρ values greater than 2 the ratio of salt flux to heat flux appears to be independent of R_ρ.

At large R_ρ values the salt-flux to heat-flux ratio begins to increase again as interface transport is dominated by diffusional transport through the core region. This trend should be expected because in the large-R_ρ region the interface thickness, as shown in figures 9–11, is essentially the same for temperature and salt. Therefore, if convective processes within the core region are assumed negligible, one would expect to find the salt-flux to heat-flux ratio given by

$$\frac{\beta F_S}{\alpha H} = \frac{\beta K_S \Delta S}{\alpha K_T \Delta T} = \tau R_\rho, \tag{3.5}$$

where $F_S \equiv$ flux of salt across interface and $H \equiv$ flux of heat across interface. Figure 13 illustrates the trend of the salt-flux to heat-flux ratio for experiment runs 13–16. The transport-ratio data shown in figure 13 have been calculated using two different methods. Shaded points use overall mixed-zone property differences as stated in (3.5). Unshaded data points use gradient information from the midplane region of the interface. The difference between shaded and unshaded data points in figure 13 is due to a deviation from linearity of one or both of the property profiles. Using gradient information, such as shown in figure 9, one finds higher transport ratios than (3.5) because the salt profile has a steep midplane gradient due to its diffusional growth.

Figure 13 also shows data in the transition region. A horizontal line above this data represents the constant property-transport level ($\beta F_S/\alpha H = 0.15$) determined by other investigators. The data in figure 13 fall significantly below this transport level because the calculation procedure only accounts for diffusional transport across the interface. One may infer that the difference between the calculated (diffusion) transport ratio and the constant-transport-ratio region is an indication of convective activity within the interface. One note of interest concerning interfaces in the

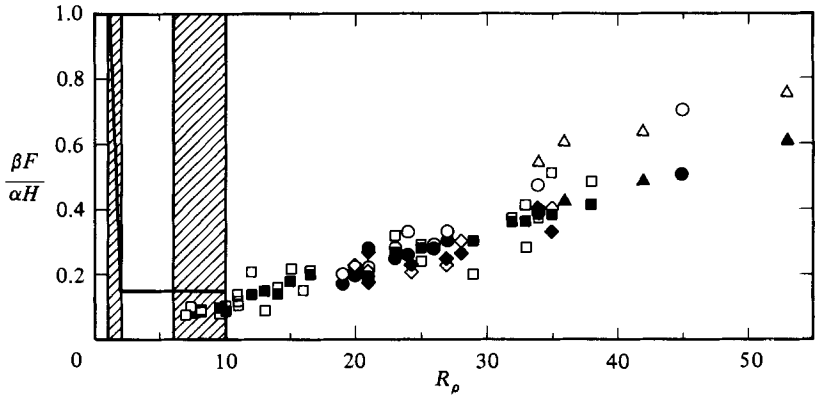

FIGURE 13. Salt-flux to heat-flux ratio for experiment runs 13, 14, 15 and 16. Shaded data were determined from (3.5). Unshaded data were determined from interface midplane salinity and temperature gradients.

transition region is that boundary-layer activity is quite significant and readily detected. Even when the traversing probe is maintained near the midplane of the interface, salinity fluctuations are often detected while temperature fluctuations are not. This occurrence may explain the reason for the constant-ratio region having a value somewhat greater than the square root diffusivity ratio. Ideally, one would expect to find a square root diffusivity ratio prediction for the transport ratio if the dominant boundary-layer processes surround a non-convecting core region. The core region may not be stable; however, the convection activity may be significant to the slower-diffusing component only. Therefore one would expect the actual transport ratio to be higher than that of ideal boundary-layer predictions.

4. Conclusions

The large-R_ρ region for a diffusive interface is a distinct regime of operation. The low-R_ρ and intermediate-R_ρ regions are distinguished by the relative levels of component transports. The intermediate-R_ρ and large-R_ρ regions can also be distinguished by the trend of component transports. Another important difference between these two regions is that the intermediate-R_ρ region is one of unique heat transport, while the large-R_ρ region can be operated under a variety of conditions resulting in varying heat-transport levels.

Erosion and growth of an interface can both occur in the large-R_ρ region. The present results indicate that regions of strong erosion and strong growth surround a region in which erosion and growth are small. That is, a relatively fast decline of interface erosion occurs as R_ρ increases past 10. The equilibrium point between erosion and growth has not yet been identified; however, a sharp transition to strong interface growth occurs as R_ρ is increased. The region of strong growth does not occur at a given value of R_ρ. The transition to strong growth appears to be similar to the region predicted by the ideal model presented.

The trends observed for the component-transport ratio are in good agreement with those expected from theoretical arguments. At large R_ρ values, and conditions near steady state, component transports are proportional to property differences across the interface. As an interface approaches intermediate R_ρ values boundary-layer processes dominate interface transport. Although no firm evidence has been reported

in this work, some core convection may be occurring at intermediate R_ρ levels, which tends to increase the transport of salt relative to heat across an interface.

The results of the present study may reveal characteristics of diffusive interfaces that undergo cyclic variations in the large-R_ρ regime, such as solar ponds. Further detailed work is required to match the present results to conditions more similar to actual solar-pond operation. It seems likely, however, that the transition region described in this work is the same operational limit observed in solar ponds. That is, as solar ponds warm up in the summer and approach the transition region, they follow a path from the non-unique operational conditions allowed in the large-R_ρ region to the unique operational path defined by the intermediate- and low-R_ρ regions.

Finally, one should note that solar ponds are not the only process in which R_ρ may be large. Oceanographical examples include the Red Sea deeps and many saline terminal lakes around the world. Solute/solute systems may also frequently operate under large-R_ρ conditions owing to more-similar diffusivity magnitudes. The sugar/salt system, for example, should transition to the large-R_ρ regime when R_ρ exceeds 1.7.

This work has been supported by the National Science Foundation under grant DME 81-05942. Also, the author would like to acknowledge the participation and efforts of Paul von Driska and Lewis Hamilton.

REFERENCES

CRAPPER, P. F. 1975 Measurements across a diffusive interface. *Deep-Sea Res.* **22**, 537–545.

HUPPERT, H. E. 1971 On the stability of a series of double-diffusive layers. *Deep-Sea Res.* **18**, 1005–1021.

HUPPERT, H. E. & LINDEN, P. F. 1979 On heating a stable salinity gradient from below. *J. Fluid Mech.* **95**, 431–464.

LEWIS, W. T., INCROPERA, F. P. & VISKANTA, R. 1982 Interferometric study of stable salinity gradients heated from below or cooled from above. *J. Fluid Mech.* **116**, 411–430.

LINDBERG, W. R. 1971 An upper bound on transport processes in turbulent thermohaline convection. *J. Phys. Oceanogr.* **1**, 187–195.

LINDEN, P. F. & SHIRTCLIFFE, T. G. L. 1978 The diffusive interface in double-diffusive convection. *J. Fluid Mech.* **87**, 417–432.

MARMORINO, G. O. 1974 Equilibrium heat and salt transport through a diffusive, thermohaline interface. M. S. thesis, Oregon State University.

MARMORINO, G. O. & CALDWELL, D. R. 1976 Heat and salt transport through a diffusive thermohaline interface. *Deep-Sea Res.* **23**, 59–67.

NEWELL, T. A. & BOEHM, R. F. 1982 Gradient zone constraints in a salt-stratified solar pond. *Trans. ASME: J. Solar Energy Engng* **103**, 280–285.

POPLAWSKY, C. J., INCROPERA, F. P. & VISKANTA, R. 1981 Mixed layer development in a double-diffusive, thermohaline system. *Trans. ASME: J. Solar Energy Engng* **102**, 351–359.

Saline Water Conversion Engineering Data Book 1971 M. W. Kellog Co., Piscataway, NJ.

SHIRTCLIFFE, T. G. L. 1969 The development of layered thermosolutal convection. *Intl J. Heat Mass Transfer* **12**, 215–222.

SHIRTCLIFFE, T. G. L. 1973 Transport and profile measurements of the diffusive interface in double-diffusive convection with similar diffusivities. *J. Fluid Mech.* **57**, 27–43.

TAKAO, S. & NARUSAWA, U. 1980 An experimental study of heat and mass transfer across a diffusive interface. *Intl J. Heat Mass Transfer* **23**, 1283–1285.

TURNER, J. S. 1965 The coupled turbulent transports of salt and heat across a sharp density interface. *Intl J. Heat Mass Transfer* **8**, 759–767.

TURNER, J. S. 1968 The behaviour of a stable salinity gradient heated from below. *J. Fluid Mech.* **33**, 183–200.